The HARPS search for Earth-like planets in the habitable zone

I – Very low-mass planets around HD20794, HD85512 and HD192310[⋆]

F. Pepe[1], C. Lovis[1], D. Ségransan[1], W. Benz[2], F. Bouchy[3,4], X. Dumusque[1], M. Mayor[1], D. Queloz[1], N. C. Santos[5,6], and S. Udry[1]

[1] Observatoire de Genève, Université de Genève, 51 ch. des Maillettes, CH–1290 Versoix, Switzerland
[2] Physikalisches Institut Universität Bern, Sidlerstrasse 5, CH–3012 Bern, Switzerland
[3] Institut d'Astrophysique de Paris, UMR7095 CNRS, Université Pierre & Marie Curie, 98bis Bd Arago, F–75014 Paris, France
[4] Observatoire de Haute-Provence/CNRS, F–04870 St.Michel l'Observatoire, France
[5] Centro de Astrofísica da Universidade do Porto, Rua das Estrelas, P–4150-762 Porto, Portugal
[6] Departamento de Física e Astronomia, Faculdade de Ciências, Universidade do Porto, Portugal

received; accepted

Abstract. In 2009 we started, within the dedicated HARPS-Upgrade GTO program, an intense radial-velocity monitoring of a few nearby, slowly-rotating and quiet solar-type stars. The goal of this campaign is to gather, with high cadence and continuity, very-precise radial-velocity data in order to detect tiny signatures of very-low-mass stars potentially in the habitable zone of their parent stars. 10 stars have been selected among the most stable stars of the original HARPS high-precision program, uniformly spread in hour angle, such that three to four of them are observable at any time of the year. For each star we record 50 data points spread over the observing season. The data point consists of three nightly observations of a total integration time of 10 minutes each and separated by 2 hours. This is an observational strategy adopted to minimize stellar pulsation and granulation noise. In this paper we present the first results of this ambitious program. The radial-velocity data and the orbital parameters of five new and one confirmed low-mass planets around the stars HD 20794, HD 85512 and HD 192310, respectively, are reported and discussed, among which a system of three super-Earths and one harboring a 3.6 $M_\oplus$-planet at the inner edge of the habitable zone. This result already confirms previous indications that low-mass planets seem to be very frequent around solar-type stars and that this occurrence frequency may be higher than 30%.

1. Introduction

During the past years the field of extra-solar planets evolved towards the exploration of very low-mass planets down to the regime of super-Earths, i.e. to objects of only few times the Earth mass. Although finding Earth-like planets is probably the main trigger for this searches, one has to consider the fact that their characterization contributes in a significant way to building up a global picture of how exoplanets form and evolve. The frequency and nature of these planets may be able to discriminate between various theories and models, deliver new inputs and constraints to them, and contribute to refining their parameters. On the other hand, the models provide us with predictions which can be verified by observations. For instance, the presently discovered low-mass planets are predicted to be only the tip of the iceberg of a huge, still undiscovered planetary population (Mordasini et al. 2009). If confirmed, hundreds of

new planets will be discovered in a near future as the radial-velocity (RV) precision improves and the various programs increase their effectiveness and their time basis.

ESO's HARPS instrument (Mayor et al. 2003) has certainly played a key role by delivering more than 100 new candidates in its first eight years of operation. The most important and impressive contribution of this instrument lies more specifically in the field of super-Earths and Neptune-mass planets. Indeed, about 2/3 of the planets with mass below 18 $M_\oplus$ known to date have been discovered by HARPS. This new era started in 2004 with the discovery of several Neptune-mass planets such as μ Ara c (Santos et al. (2004), see also Pepe et al. (2007) for an update of the parameters), 55 Cnc (McArthur et al. 2004), and GJ 436 (Butler et al. 2004). Many more followed, but the detection of the planetary system HD 69830 containing three Neptune-mass planets (Lovis et al. 2006), and that of HD 40307 with its three Super-Earths (Mayor et al. 2009b), best illustrate the huge potential of HARPS. HARPS also revealed to us the system Gl 581, with two possibly rocky planets c and d having masses of 5 and 8 M-Earth, respectively, both lying at the edge of the habitable zone (HZ) of their parent star (Udry et al. 2007; Selsis et al. 2007), and the Gl 581 e of only 1.9 $M_\oplus$ (Mayor
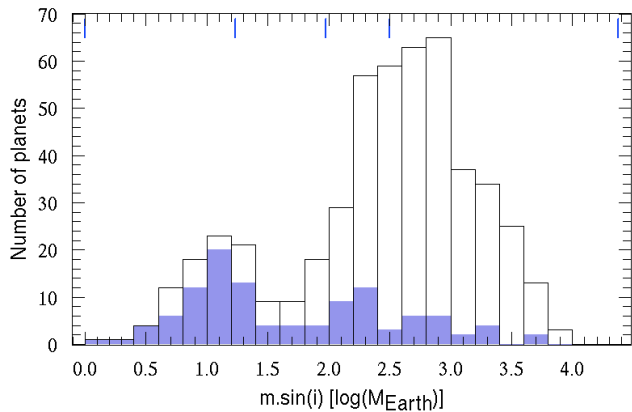
Fig. 1. Histogram of companion masses. The dark area shows the companions discovered with HARPS and includes the candidates which are in preparation for publication.

et al. 2009a). Last but not least, we should mention the system around HD 10180, with 7 extra-solar planets of low mass, among which the lightest ever detected exoplanet HD 10180 b, with $m * \sin i$ of only $1.5\,M_\oplus$ (Lovis et al. 2011b).

Figure 1 shows the mass distribution of companions around solar-type stars of all the published planets, including the HARPS candidates which are in preparation. The HARPS detections (dark area) probe a mass range which suffered from strong detection biases before. It must be noticed that the planet frequency increases again below $20\,M_\oplus$. This increase is highly significant, since higher-mass planets induce higher RV variations on their parent star and are therefore detected more easily. Moreover, a recent investigation of the HARPS high-precision sample has shown that about 1/3 of all sample stars exhibit RV variations indicating the presence of super-Earths or ice giants (Lovis et al. 2009). Indeed, planet formation models (Ida & Lin 2008; Mordasini et al. 2009; Alibert et al. 2011) show that only a small fraction (of the order of 10%) of all existing embryos will be able to grow and become giant planets. *Hence, we expect that the majority of solar-type stars will be surrounded by low-mass planets.* The inclusion of telluric planets can only increase further the planet frequency and thus the probability of detection. This implies that even a small sample of target stars is likely to reveal, if followed with high enough accuracy, several Earth-like planets. Pushing the measurement precision further should therefore naturally increase the probability of finding new planets, especially of very low mass and rocky, and possibly in the habitable zone of their host star.

In the following section we will describe our program for the specific search for low-mass and rocky extra-solar planets lying possibly in the habitable zone of their parent star. The observations of these targets is presented in Section 3. The three host stars of the program around which we have detected new planets will be described in greater detail in Section 4. Section 5 presents the three newly discovered planets as well as the confirmation of a recently announced planet. Finally, a short discussion and an outlook on the occurrence frequency of low-mass planets is given in Section 6.

2. Searching for Earth analogs around nearby stars

The recent HARPS discoveries made us aware of the fact that discovering Earth-like exoplanets is already within the reach of HARPS, although important questions still remain open: How frequent are low-mass planets? At what level is the detection bias? Where is the precision limit set by stellar noise? Can we detect low-mass planets in the habitable zone of their parent star if sufficient observations on a high-precision instrument are invested? Driven by the very encouraging results of the HARPS High-Precision programme (Udry & Mayor 2008) and the hints for high planet occurrence announced by Lovis et al. (2009), we have decided to investigate these questions in further detail. For this purpose, we have defined a specific program on HARPS for the search of rocky planets in the habitable zone HZ based on Guaranteed Time Observations (GTO).

We decided to observe 10 nearby stars with the highest possible radial-velocity precision and sampling during a period of 4 years. Our goal is to probe the presence of extra-solar planets as similar as possible to our Earth. Therefore, we have selected targets with the following characteristics:

- The stellar magnitude must be such that we are not limited by photon noise within a 15-minutes exposure, i.e. ensure an RV-precision of better than $30\,\mathrm{cm\,s^{-1}}$.
- Stars should lie within 10 pc from the Sun.
- The targets must have characteristics which guarantee the best RV precision, i.e they should be of late-G to early-K spectral type and have low rotational velocity (a rotational velocity below what can be detected with HARPS, i. e. $v \sin i < 1\,\mathrm{km\,s^{-1}}$) and low activity indicators ($log(R'_{HK}) < -4.85$).
- The RV scatter measured with HARPS over the first years of operation must be lower than 2 m/s rms over several years and based on a minimum of 10 recorded data points.
- The ten targets must be evenly distributed in terms of right-ascension to allow the observation of at least 3 to 4 targets at any period of the year.

Combining all these criteria resulted actually in a strong down-selection of the 400 possible candidates of the original HARPS high-precision program. In particular the requirement on the distance from the Sun resulted to be too limiting, when considering all the other requirements, such that we had to relax this requirement and allow targets to enter the list with distances up to 16 pc.

The 10 selected targets are given in Table 1. The most prominent member is Alpha Cen B (HD 128621). This star is of particular interest because of its brightness and its short distance to the Sun. If planets were detected around Alpha Cen B they would be ideal candidates for further follow-up by spectroscopy, astrometry, photometry, etc. Furthermore, this star is part of a triple system which makes the question even more interesting. However, what appears to be the greatest advantage generates some observational challenge: On the one hand, the bright magnitude of Alpha Cen B is a limiting factor for the telescope guiding system and may result in poorer RV precision due to incomplete light scrambling across the spectro-

Table 1. Targets of the HARPS' search for Earth analogs around nearby stars program

Target	R.A. [h:m:s]	DEC [°:':"]	Sp. type	*V*Mag	Dist. [pc]
HD 1581	00:20:04	-64:52:29	F9V	4.23	8.59
HD 10700	01:44:04	-15:56:15	G8V	3.49	3.65
HD 20794	03:19:55	-43:04:11	G8V	4.26	6.06
HD 65907A	07:57:46	-60:18:11	G2V	5.59	16.19
HD 85512	09:51:07	-43:30:10	K5V	7.67	11.15
HD 109200	12:33:31	-68:45:20	K0V	7.13	16.17
HD 128621	14:39:35	-60:50:14	K1V	1.35	1.35
HD 154577	17:10:10	-60:43:43	K0V	7.38	13.69
HD 190248	20:08:44	-66:10:55	G5IV-V	3.55	6.11
HD 192310	20:15:17	-27:01:58	K3V	5.73	8.82

graph's entrance slit. On the other hand, Alpha Cen B being in a triple system, the RVs must be analyzed by considering a complete - and precise - orbital model, especially when looking at long-period planets.

Another prominent candidate is τ Ceti (HD 10700). This star was already known to be a 'RV-standard' star in the sense that it is followed up by several groups and shows a very low RV dispersion. Indeed, the RV dispersion measured with HARPS over a time span of more than 7 years and involving 157 data points is of 0.93 ms! Because of its magnitude, the spectral type, the RV stability and its low chromospheric activity level, τ Ceti is close to the perfect candidate for our program.

The remaining 8 candidates show similar characteristics. They are all part of the original HARPS high-precision program. As such, they have all been being observed since the very beginning of the HARPS operations, a fact that allowed us to make a preliminary selection also on the basis of preliminary RV-dispersion and chromospheric activity indicator values. Since the start of our specific program on April 1st, 2009, the number of measurements has increased and the mentioned values refined.

An important aspect to be pointed out, is that the presented program carries some 'risks': By construction this program pre-selected only very stable stars in terms of radial velocities. In other terms, we were sure that they would not harbor any *known* planet. Even worse, their raw RV dispersion does not leave much room for 'large' RV signals. Of course, we were conscious of this fact and that we might end up with no positive result.

There is no doubt that successful detections depend on the observational precision, in particular when searching for signals with semi-amplitudes below 1-2 m s^{-1}, as it is the case for the presented program. Five years of observations have proved that, on quiet and bright dwarf stars, a radial-velocity precision well below 1 m s^{-1} can be achieved on both short-term (night) *and* long-term (years) timescales. A direct confirmation is offered by the raw RV dispersions measured for the candidates of our program and given in Table 2.

In order to make a rough estimation of the detection limits we may expect, let us assume a precision of 0.7 m s^{-1} on each data point all included, i.e. stellar noise, instrumental errors,

atmospheric effects, etc. The photon noise is 'by design' well below this level and can be neglected. With 50 well-sampled data points we should then be able to detect a 50 cm s^{-1} RV semi-amplitude at better than a 3-sigma level. This signal corresponds to a 2.2 $M_\oplus$ on a 1-month orbit or a 4 $M_\oplus$ on a 6-months orbit. When extended to 3 years, the same observational strategy will allow us to increase the number of data points and consequently reduce the detectable semi-amplitude to about 30 cm s^{-1} or the equivalent of a 1.3 $M_\oplus$ planet on a 1-month orbit, or a 2.3 $M_\oplus$ on a 6-months orbit. On the other hand, it is interesting to note that such a planet would lie at the inner edge of the habitable zone of Alpha Cen B or even inside the habitable zone of HD 85512 or HD 192310, which are later-type stars.

In the previous discussion it was assumed of course that no RV signal induced by stellar activity is present at the orbital period of investigation. In the opposite case, the detection limit will not decrease proportionally to the square-root of the number of data points. Even worse, if the stellar activity signal has a coherence time similarly or longer than the observational period, it becomes indistinguishable from a possible radial-velocity signal of similar periodicity. However, other indicators such as precise photometry of the star, line bisector or stellar activity indicators can help to identify possible correlations with the radial-velocity signal and thus provide a tool to distinguish stellar noise from a planetary signal. Another powerful tool is to verify that the RV signal is persistent and coherent over time.

3. Observations

3.1. HARPS-Upgrade GTO

All the observations presented in this paper have been carried out using HARPS on ESO's 3.6-m telescope at the La Silla Observatory, Chile (Mayor et al. 2003). A total of 30 nights per year over 4 years are allocated to this program on HARPS within our Guaranteed-Time Observations (HARPS-Upgrade GTO). Our goal was to observe each target about 50 times per season. These constraints, together with the need of observing each target several times per night in order to average stellar noise, set the actual number of targets we are able to follow-up. In the following we shall discuss the observational strategy. For this purpose we have to distinguish different types of measurements and adopt following definitions: An *exposure* represents the single integration (one open-close shutter cycle). The *observation* is the average of all subsequent exposures. The *data point*, finally, shall denominate the average of all the exposures in a given night.

3.2. Observational strategy

Thanks to the experience issued from the HARPS high-precision program we have been able to define an optimum strategy of observation to reduce the effects of stellar noise and its impact on the RV measurements. From the study by Dumusque et al. (2011b) we have learned that stellar pulsations are best averaged out by extending the measurement over

a time longer than the typical stellar oscillation period. Since our targets are mainly bright G and K dwarfs, we ended up with exposure times of typically 15 minutes. In order to avoid saturation on bright objects, the exposures where split in several shorter exposures covering a total of 15 minutes, including overheads, leading to typical 'open-shutter' time of about 10 minutes. From the same study we can also deduce that super-granulation noise, being of longer time scale, is not averaged out by the 15-minutes exposure. For this purpose, the daily time scale must be covered. This led us to observe each target at least twice, if possible 3 times during the same night, but in any case with the single observations separated as far as possible in time. A total observation time per target of 35-45 minutes per night had to be considered. If we assume 10 hours per night in average, we end up with about 40 to 50 possible observations per target and per year.

Dumusque et al. (2011b) show that longer-period granulation noise and RV-jitter due to spots and activity are best averaged out by sampling evenly the observational season. If we fix the amount of available observation time, an equidistant time grid would be the best solution. However, the visitor-observing scheme applied to ESO's 3.6-m telescope does not allow us to obtain optimum sampling. Nevertheless, it has been possible to join our GTO time with observations of other large programs. The result is that, during nights allocated to this joint program, about two to three targets are observed in average every night, while no data are obtained during other nights, leaving some observational gap with a typical period of one to few weeks.

3.3. Obtained measurements

Table 2 summarizes the measurements made with HARPS on each of the program's targets, including measurements issued from the original high-precision program. The second column indicates the number of data points (nightly averages of individual exposures) acquired to date. Thanks to the data-points of the original high-precision program, most of the observations span over more than 6 years for any of the objects. It must be noted however, that the first-years observations on HARPS were not carried out using the optimum observational strategy, resulting in data points – actually single exposures – of poorer precision. Despite this, the RV scatter of all these data points is remarkably low, justifying our initial choice of the targets. The only target for which the RV scatter exceeds $1.5\,\mathrm{m\,s^{-1}}$ is HD 192310. Interestingly, this star has been recently announced by Howard et al. (2010a) to harbor a Neptune-mass planet. The discovery is actually confirmed by the HARPS data and will be described in further detail in Section 5. The RV scatter of Alpha Cen B (HD 128621) is not indicated in the table, since it is affected by the long-term drift caused by its stellar companion. A detailed discussion specific to Alpha Cen B will be presented in a forthcoming paper. For all targets we give the value of the chromospheric activity indicator $\log(R'_{\mathrm{HK}})$. As mentioned in previous sections, the targets where selected to have $\log(R'_{\mathrm{HK}}) < -4.85$. The long-term averages and the dispersion values given in the last column confirm that all the targets comply with this requirement.

Table 2. Observations of the targets with HARPS

Target	Data points	Time span [days]	RV scatter [m s^{-1}]	$\log(R'_{\mathrm{HK}})$
HD 1581	93	2566	1.26	-4.93 ± 0.003
HD 10700	141	2190	0.92	-4.96 ± 0.003
HD 20794	187	2610	1.20	-4.98 ± 0.003
HD 65907A	39	2306	1.45	-4.91 ± 0.006
HD 85512	185	2745	1.05	-4.90 ± 0.043
HD 109200	77	2507	1.16	-4.95 ± 0.018
HD 128621	171	2776	NA	-4.96 ± 0.014
HD 154577	99	2289	1.05	-4.87 ± 0.026
HD 190248	86	2531	1.26	-5.09 ± 0.009
HD 192310	139	2348	2.62	-4.99 ± 0.033

3.4. The example of Tau Ceti

In order to illustrate the kind of objects we are dealing with and the level of precision which can be obtained with HARPS, we shall focus a moment on HD 10700, also known as Tau Ceti. The dispersion over the RVs of the *individual exposures* (typically a few minutes) is of $1.5\,\mathrm{m\,s^{-1}}\,rms$. As seen in Table 2, the dispersion of the data points *(nightly averages)* is instead only $0.92\,\mathrm{m\,s^{-1}}$, which proves that the strategy proposed by Dumusque et al. (2011b) provides good smoothing of the stellar contributions at the time scale of a night. HD 10700 results to be part of the most quiet stars in our sample despite the large number of data points spanning more than 6 years of observations. What is even more remarkable it that none of the parameters shown in Figure 2, i.e. the radial velocity, the chromospheric activity indicator $\log(R'_{\mathrm{HK}})$, and the average line bisector of the cross-correlation function BIS, show any trend over the 6 years of observations. For instance, the activity indicator shows a dispersion of only 0.003 dex *rms*. Finally, we shall underline the stability of the line bisector, which has a dispersion of about $0.5\,\mathrm{m\,s^{-1}}$, confirming the high stability of HARPS' instrumental profile (IP).

In the upper panel of Figure 3 we plotted the Generalized Lomb-Scargle (GLS) periodogram of the radial velocity data of HD 10700. Note that none of the peaks reaches the 10% false-alarm probability (FAP) level. This demonstrates that there is not any significant planetary signal in the precise HARPS data available to date and we can set a higher limit for the masses of possible planets aroun Tau Ceti as a function of period. For a detailed analysis and discussion we refer to Lovis (2011).

In the central and lower panel of Figure 3 we present the GLS periodogram of the $\log(R'_{\mathrm{HK}})$ and the line bisector BIS. The peaks are here significant, opposite to the RV data, and indicate that there is some 'signal' which is clearly above the noise. Periodograms of activity indicators like $\log(R'_{\mathrm{HK}})$ and line bisector BIS often exhibit a complicated pattern of significant peaks around the stellar rotation period and at longer periods. This can probably be explained by the combination of irregular sampling and the presence of signals with short coherence times in the data, as expected from stellar activity and spots. Indeed, solar-type stars are likely covered by a large number of small active regions which rotate with the star and have lifetimes of the order of the rotation period or below. The
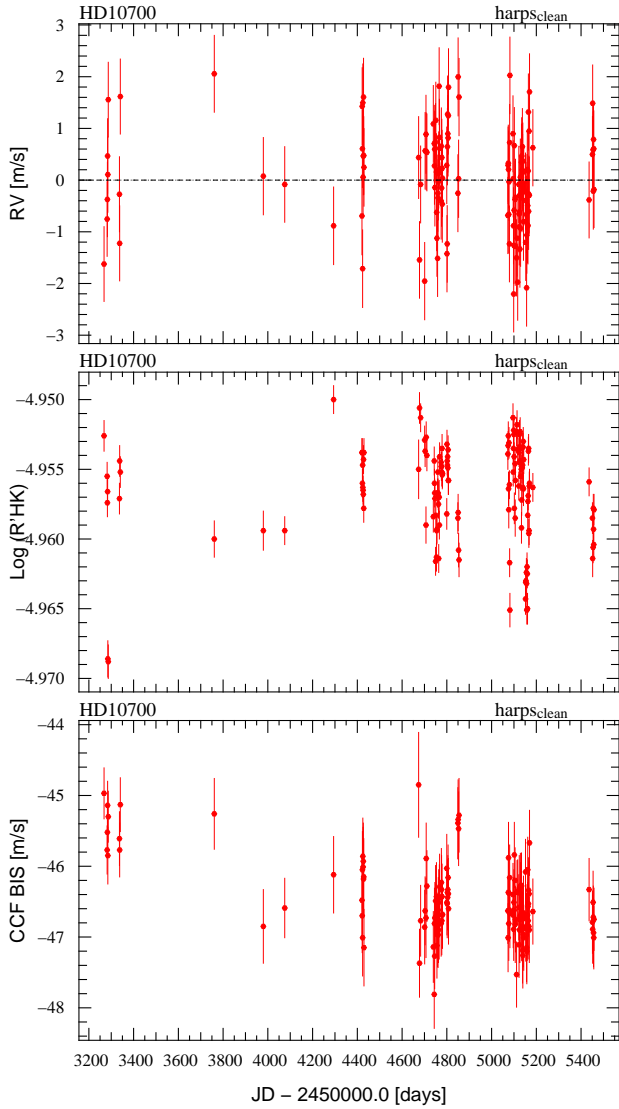
Fig. 2. Radial velocities, chromospheric activity indicator $\log(R'_{HK})$, and line bisector $CCF\,BIS$ of HD 10700 versus time

Fig. 3. GLS periodograms of the HD 10700 radial velocities (upper panel), its $\log(R'_{HK})$ values (central panel) and line bisector *BIS* (lower panel). The false-alarm probability (FAP) thresholds of 10% is indicated by a dashed line.

quantities is plotted. We deduce that in the specific case of Tau Ceti, the radial velocity is not affected by stellar activity.

HD 10700 is thus a star that shows no detectable coherent signal in the RV data, while activity indicators exhibit some non-random, low-amplitude patterns that likely convey information on small active regions at the stellar surface. In this sense, these indicators are more sensitive to activity than RV data, which make them useful tools to better understand stellar jitter on quiet solar-type stars. Work is going on to simulate and model these auxiliary data, which may then allow us to eventually correct the RV data themselves from activity effects.

4. Parameters of the planet-hosting stars

Of the ten targets presented in the previous section, three of them presently show planetary signatures. The stars are HD 20794, HD 85512 and HD 192310. The target HD 192310 was already announced recently by Howard et al. (2010a) to harbor a Neptune-mass planet on a 74 days orbit. In the following we will confirm this detection and show that a second planet orbits this star on a much longer orbit.

The photometric and astrometric parameters of the three targets are presented in the first part of Table 3. They are all obtained from the HIPPARCOS catalog (ESA 1997). Given the fact that all targets are nearby stars, also the astrometric parameters are very precise.

The spectroscopic parameters presented in the second part of Table 3 have been collected from Sousa et al. (2008), who did a in-depth spectroscopic analysis of all stars of the HARPS

aspect to be pointed out here, however, is that these peaks do not have any correspondence in the RV GLS periodogram. As remarked previously, the (low but significant) activity signal is not correlated to any RV variation.

One may also wonder how strongly stellar activity may influence the radial-velocities. We refer to Dumusque et al. (2011a) and Lovis et al. (2011a) for a detailed discussion. In the specific case of Tau Ceti we observe only little RV jitter despite the fact that the $\log(R'_{HK})$ seems to vary during some seasons, while it remains stable over others. As an example, Figure 4 shows the radial velocity, $\log(R'_{HK})$ and *BIS* over a single season. Error bars on $\log(R'HK)$ values have been calculated from the expected photon statistics, but in order to take into account the effective noise floor (determined on the most stable stars) an uncertainty of 0.001 was quadratically added. This noise floor is likely due to residual instrumental systematics. The variation in $\log(R'_{HK})$ is larger than the expected error, but does not seem to follow the radial velocity, and vice-versa. This is better illustrated in Figure 5 where the correlation between the two
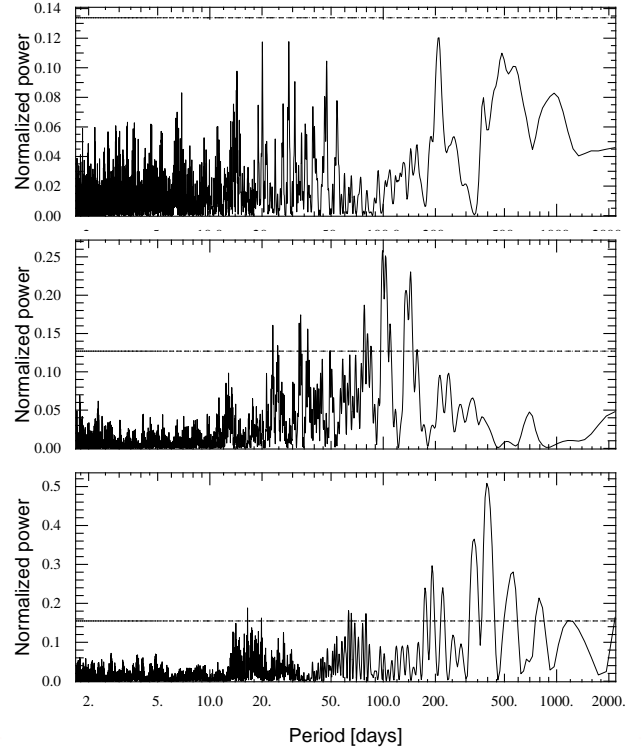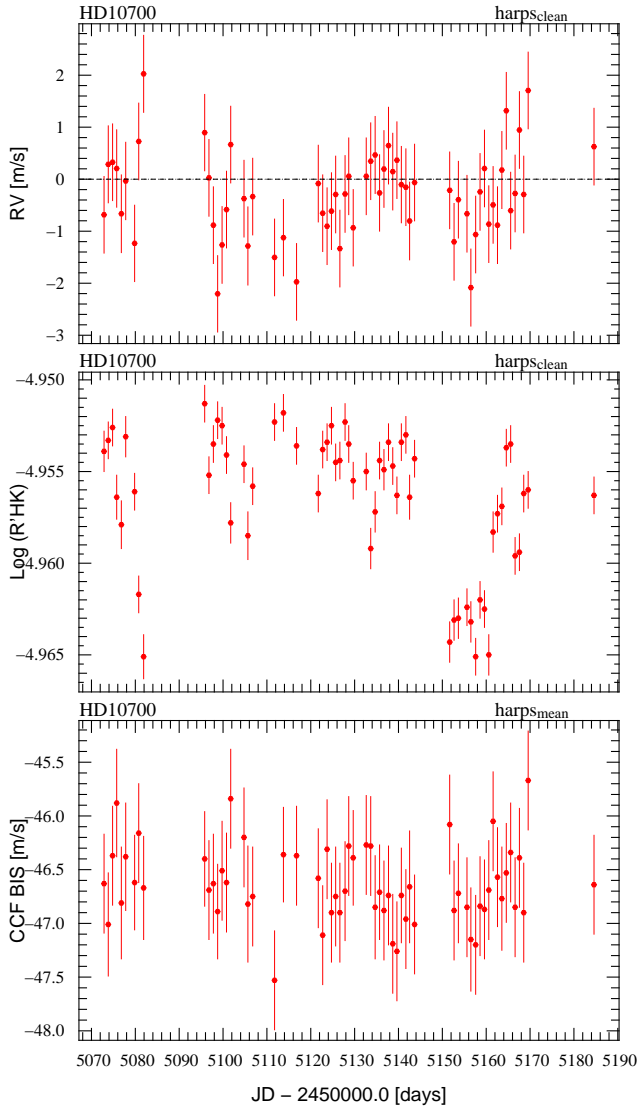
Fig. 4. Radial velocitiy, chromospheric activity indicator $\log(R'_{HK})$ and line bisector *BIS* of HD 10700 over a single season

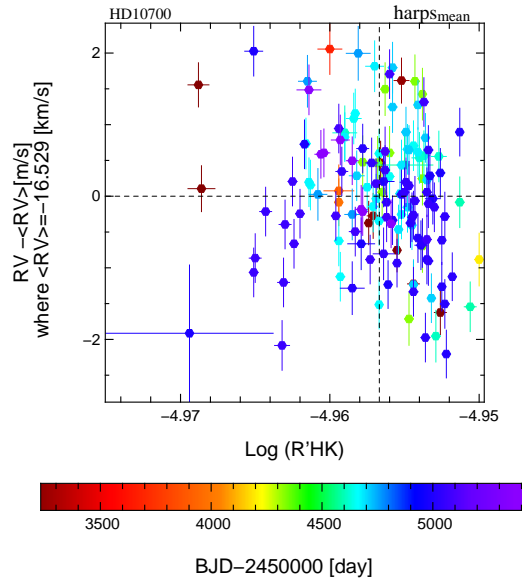**Fig. 5.** Correlation plot of radial velocity versus chromospheric activity indicator $\log(R'_{HK})$ for HD 10700. The color scale represents the observation date.

high-precision program. We report them here without any further analysis. We shall only comment that for the K5V dwarf HD85512 the stellar parameters derived in Sousa et al. may be affected by systematic errors (see e.g. Neves et al. 2009), given the late spectral type of the star. In fact, Sousa et al. (2008) derived an effective temperature of 4715 ± 102 K for this star, in disagreement with the value of 4419 K obtained using the IRFM calibration of Casagrande et al. (2006).

To check if this difference could significantly change the derived stellar metallicity and estimated stellar mass, we proceeded with a series of tests. First, fixing the effective temperature to 4419 K and the gravity and microturbulence values derived by Sousa et al. (4.39 dex and 0.23 km s^{-1}, typical for late K-dwarfs), we derived a new value for the stellar metallicity based on the list of Fe I lines (and their equivalent widths) measured by Sousa et al. The resulting [Fe/H] is -0.34, very close to the original value of Sousa et al. Finally, we estimated the stellar mass using both effective temperature values mentioned above, and making use of the Mass–T_{eff}–$\log g$–[Fe/H] calibra-

tion of Torres et al. (2010). In this procedure we fixed the stellar metallicity to -0.32 and the gravity to 4.39, while attributing reasonable (though conservative) uncertainties of 0.1 and 0.2 dex to [Fe/H] and $\log g$, respectively. The error in effective temperature was considered to be 100 K in each case. After a series of 10'000 Monte Carlo trials, using values of T_{eff}, $\log g$, and [Fe/H] taken from a Gaussian distribution around the central value and a dispersion of 1-sigma (error), we obtained mass values of 0.73 and 0.65 $M_\odot$ for input temperatures of 4715 and 4419 K, respectively (the uncertainly is 0.08 $M_\odot$, taking into account the scatter of the individual mass values and the dispersion of the Torres et al. calibration). Both values are compatible within the error bars. The former value is close to the 0.74 $M_\odot$ derived by Sousa et al. through isochrone fitting. We thus conclude that both [Fe/H] and mass values are not strongly sensitive to the choice of the effective temperature scale. We decided to adopt in the remaining of the paper the average value of the two: -0.33 for [Fe/H] and 0.69 $M_\odot$ for the mass of HD85512.

The third part of Table 3 shows eventually a series of other stellar parameters: The projected stellar rotation velocity is issued from the instrumental calibration presented by Santos et al. (2002). The chromospheric activity indicator. $\log(R'_{HK})$ has been computed in accordance with Lovis (2011). Finally, the stellar rotation period $P_{rot}(R'v_{HK})$ and the estimated stellar age are both computed from $\log(R'_{HK})$ following the prescription given in Mamajek & Hillenbrand (2008).

Table 3. Observed and inferred stellar parameters for the observed targets.

Parameter		HD 20794	HD 85512	HD 192310
Spectral Type		G8V	K5V	K3V
V		4.26	7.67	5.73
$B - V$		0.711	1.156	0.878
V variability		< 0.005	< 0.016	< 0.005
π	[mas]	165.02 ± 0.55	89.67 ± 0.82	113.33 ± 0.82
Distance	[pc]	6.06	11.15	8.82
pmRA	[mas/yr]	39.21 ± 0.44	461.28 ± 0.56	1241.35 ± 0.78
pmDEC	[mas/yr]	27.57 ± 0.45	-472.87 ± 0.57	-181.46 ± 0.51
M_V		5.35	7.43	6.00
L	[$L_\odot$]	0.656 ± 0.003	0.126 ± 0.008	0.385 ± 0.007
$[Fe/H]$	[dex]	-0.40 ± 0.01	-0.33 ± 0.03	-0.04 ± 0.03
M	[$M_\odot$]	0.70	0.69	0.80
T_{eff}	[K]	5401 ± 17	4715 ± 102	5166 ± 49
$\log g$	[cgs]	4.22 ± 0.11	4.39 ± 0.28	4.51 ± 0.09
$v \sin i$	[km s^{-1}]	< 3	< 3	< 3
$\log(R'_{\mathrm{HK}})$	[dex]	-4.976 ± 0.003	-4.903 ± 0.043	-4.994 ± 0.027
$P_{\mathrm{rot}}(R'v_{\mathrm{HK}})$	[days]	33.19 ± 3.61	47.13 ± 6.98	47.67 ± 4.88
age(R'_{HK})	[Gyr]	5.76 ± 0.66	5.61 ± 0.61	7.81 ± 0.90

5. Results and orbital solutions

5.1. The planetary system of HD 20794

The raw radial-velocity data of the star HD 20794 are shown in Figure 6. As it can be seen from these raw data the star belongs to the most stable stars of the original HARPS high-precision sample. The dispersion of the 173 radial-velocity data points is of only 1.2 m s^{-1} rms over the 7-years time span. The typical internal noise on the radial velocity data points, which takes into account photon and calibration noise, is of 0.2 to 0.3 m s^{-1}. For the analysis, and in order to take into account any possible external noise such as instrumental, atmospheric and stellar contaminants, as well as stellar jitter, we add quadratically a systematic noise of 0.7 m s^{-1} to the RV data. This value considers the typical dispersion obtained for the most stable stars of the program and prevents that some high SNR data are erroneously over-weighted with respect to others in the fitting process.

Although low, the dispersion largely exceeds the estimated total error. The GLS periodogram shows indeed a signal well above the noise level at about 18 days period (see Figure 7). The dashed line indicates a false-alarm probability level of 1% but the $P = 18$ days signal exceeds this level by far. In the same figure we plot for comparison the GLS periodogram of the activity indicator $logR'_{HK}$ and of the line bisector BIS. None of them reveal any significant power at the period indicated by the radial velocity. The $\log(R'_{\mathrm{HK}})$ indicator and the bisector, instead, show an excess of power at periods around 30 days, which points towards the rotational period of this star. Since the periods are significantly different from the radial-velocity period, we conclude that the two signals are de-correlated. Nevertheless, it must be noted that $\log(R'_{\mathrm{HK}})$ has a significant peak at $P = 32$ days, which we suppose reflecting the stellar rotational period. Remarkably, this value perfectly corresponds to the value directly computed from $\log(R'_{\mathrm{HK}})$ using the Mamajek & Hillenbrand (2008) prescriptions.

Based on the clear $P = 18$ days signal issued from the periodogram, and reassured by the non-coincidence of the $\log(R'_{\mathrm{HK}})$ and BIS peaks with the radial-velocity peak, we have fitted a single Keplerian to the radial velocities while letting all the parameters free. The period of the obtained solution converges very rapidly and unambiguously towards a period of about 18 days, a semi amplitude around 1 m s^{-1}, and an eccentricity of 0.25. However, since the eccentricity error is of the same order as its value, and since the residuals almost do not depend on the eccentricity, we have decided to fix it to zero. For the $N = 187$ data points we obtain a residual dispersion around the proposed solution of 1.03 m s^{-1}. The reduced χ^2 is thus of 2.06, indicating that some excess dispersion exists and must be due to an additional signal or an external noise source, e.g. additional stellar noise, as suggested by the excess power in the $\log(R'_{\mathrm{HK}})$ and line-bisector spectra. The GLS periodogram of the residuals to the one-Keplerian fit (center of Figure 8) indeed indicates excess power around 90 days with a false-alarm probability well below 1%. This signal is not correlated with $\log(R'_{\mathrm{HK}})$ or BIS and the fact is confirmed when computing the Pearson's correlation coefficients which is in both cases close to zero.

Encouraged by the significance of the two signals at 18 and 90 days and the absence of any correlation with the activity indicator and the line bisector, we have decided to try a two-Keplerian model to fit our data. For the first run we left all the parameters free. The obtained solution is quite convincing but the eccentricities are not significantly different from zero. Therefore, we have fixed them to zero in the second run. The two-Keplerian model with zero eccentricities delivers two planets with a period of 18 and 90 days, both having a semi-amplitude of about 0.8 m s^{-1}. The residual dispersion of the data points around the fit is 0.90 m s^{-1} and χ^2 is equal to 1.61. It is interesting to note that the residuals to this solution still contain significant power at $P = 40$ days. This fact is illustrated by the presence of a significant peak in the third plot of Figure 8,
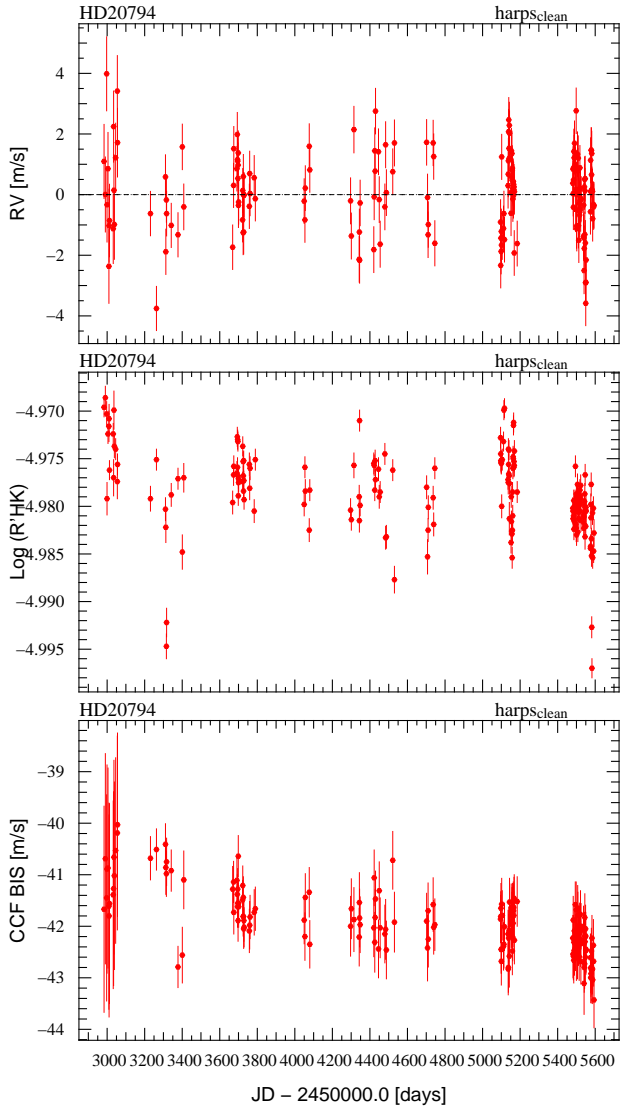
Fig. 6. Radial velocity, $\log(R'_{HK})$ and *BIS* of HD 20794 as a function of time. The RV dispersion is of 1.23 m s^{-1} *rms*.

Fig. 7. GLS periodogram of the HD 20794 radial-velocity data with FAP levels at 10% and 1% level, respectively (top), the activity indicator $\log(R'_{HK})$ (center) and the line bisector *BIS* (bottom). While a very clear peak appears at $P = 18$ days for the radial velocities, no such signal is seen in the two other observables.

which dominates with an FAP of 0.7%. It must be said, however, that the peak is strongly attenuated if the eccentricities of the two planets are let free, probably because the eccentricity of the two Keplerians 'absorb' part of the 40 days-period signal. Opposite, one could argue that a real non-zero eccentricity of the longer-period planet, if not taken into account in the fitted model, would rather produce harmonics. We would expect a signal around half the longer period, i.e. 45 days. The period of the peak in the residuals is significantly different, however. We conclude therefore that some additional contribution at $P = 40$ days may still be present in the data, which has not been taken into account by the two-Keplerian model. Furthermore, the 40 days peak in the GLS periodogram does not appear to have a corresponding peaks neither in the activity indicator nor in the line bisector. This is well confirmed by the correlation plots in Figure 9 showing a Pearson correlation coefficients of only 0.06 between RV and activity indicator and of 0.15 between RV and line bisector.
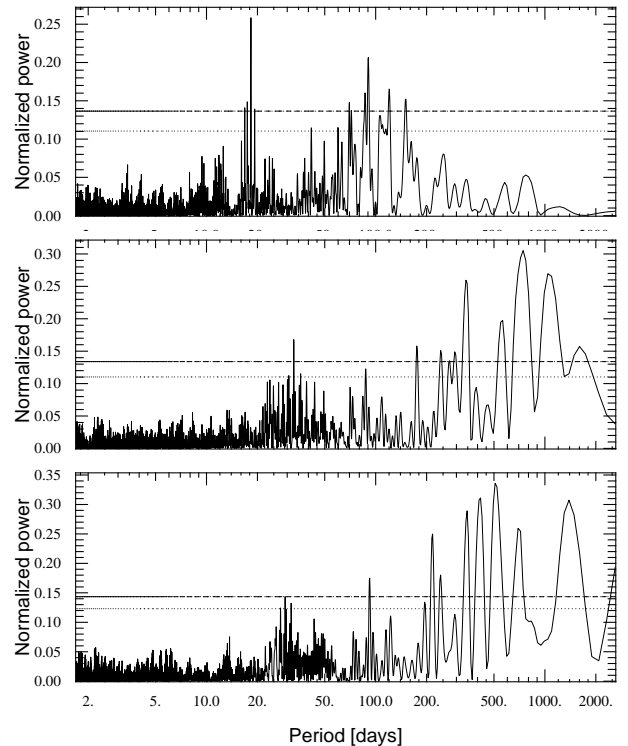
We studied the distribution of the RV residuals to both models (eccentric 2-planet and circular 3-planet) as a possible way to discriminate between them (see e.g. Andrae et al. (2010)). Unfortunately, both models yield distributions of normalized residuals close to Gaussian, and the Kolmogorov-Smirnov test gives similarly high probabilities that the residuals are drawn from a normal distribution (97% and 80% for the 3-planet and 2-planet models, respectively). Note that this result depends on the assumed level of jitter, and that reducing the error bars increases the difference between the models in favor of the 3-planet model. However, it is hardly possible to choose between the models on this basis. Gathering more data may be the only way to confirm the existence of the third planet.

All these considerations lead us to adopt a three-Keplerian model. The resulting orbital parameters are presented in Table 4. The corresponding phase-folded radial-velocity curves are shown in Figure 10. As mentioned before, the eccentricities were fixed to zero, but only after searching for generic solutions and verifying that the eccentricity values were not significant. The semi-amplitudes of the induced radial-velocity variation are *all* lower than 1 m s^{-1}. The orbital periods of the three components are at 18, 40, and 90 days.

The shortest and longest-period signal are very significant, while the $P = 40$ days period is well detected in the periodogram but is less apparent in the phase-folded RV plot. Given the low amplitude, which would be the lowest ever detected radial-velocity variation induced by a planet, and the fact that
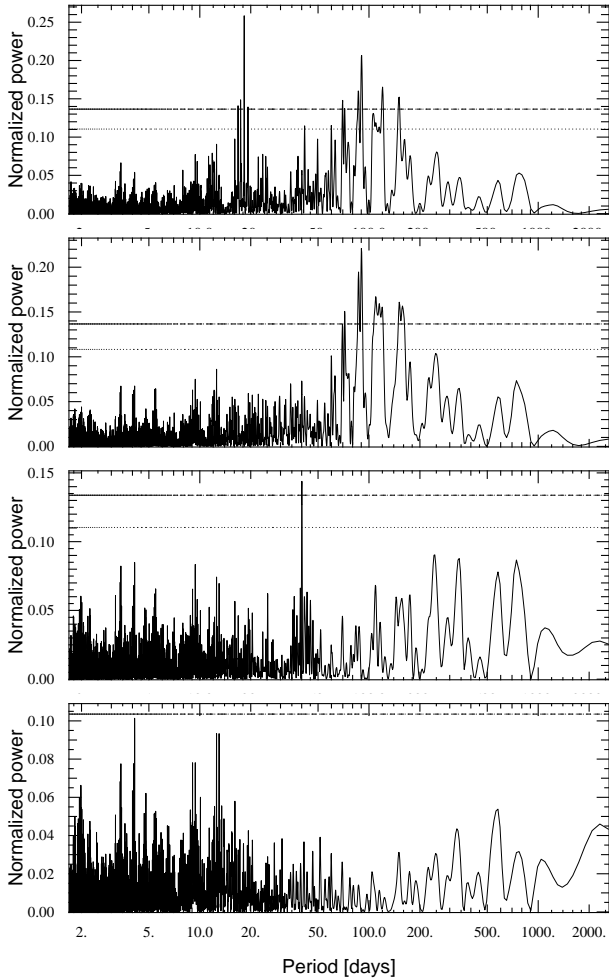
Fig. 8. Successive GLS periodograms of the HD 20794 time series, where the main signal is subtracted at each step by adding one more planet in the multi-Keplerian model from top to bottom, starting from the GLS of the raw data and following with the residuals to the one-Keplerian and the two-Keplerian fit. Eccentricities have been set to zero. False-alarm probability thresholds of 10% and 1% are indicated. The lowest GLS periodogram of the residuals to the three-Keplerian model shows only the 10% FAP level.

the orbital period is close to the supposed rotational period of the parent star, we remain prudent with this third candidate. In the frame of our program we will continue observing this star to possibly confirm the planetary nature of the c component.

The semi-major axis of the planetary orbits are 0.12 AU, 0.20 AU and 0.35 AU. For the minimum mass of the planets we obtain $m_b \sin i = 2.68 [M_\oplus]$, $m_c \sin i = 2.38 [M_\oplus]$ and $m_d \sin i = 4.72 [M_\oplus]$. We end up with three Super-Earths in the same system. The error on the mass due to only the fit uncertainties is of the order of 10% and 15%, respectively, very similar to the error set by the uncertainty on the stellar mass. It is worth noting that this system is of exactly the nature we were looking for, i.e. low-mass (possibly rocky) planets on not too close orbits. However, even for the furthermost planet d, the equilibrium temperature defined by a Bond albedo of 0.3 is of the order of 388 K (see Selsis et al. (2007) for details on the definition and estimation of equilibrium temperature).
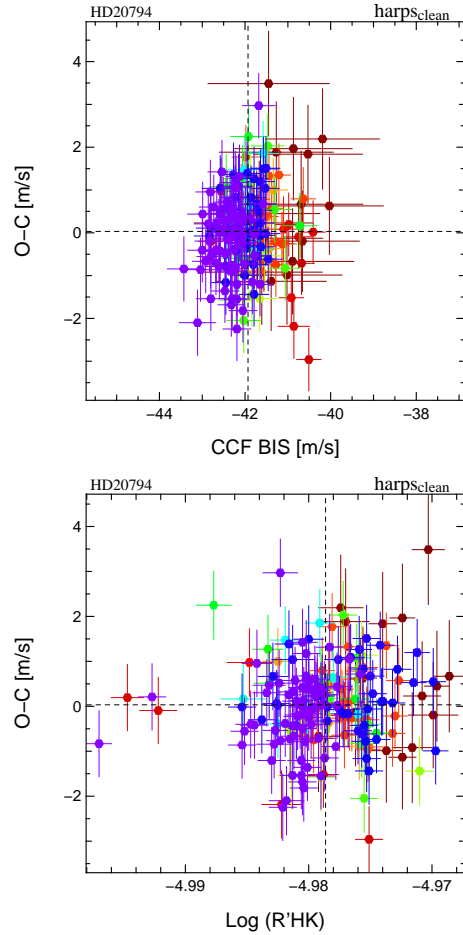

Fig. 9. Correlation plot of the residual of the two-Keplerian model to the radial velocity of HD 20794 versus the line bisector and the activity indicator $\log(R'_{\mathrm{HK}})$, respectively

5.2. The planetary system around HD 85512

The raw radial-velocity data of the star HD 85512 are shown in Figure 11. By initial choice this star is among the most stable stars of the original HARPS high-precision sample. The dispersion of the 185 radial-velocity data points is, with $1.05 \, \mathrm{m\,s^{-1}} rms$ over the 7.5-years time span, below that of HD 20794. The typical internal error on the radial velocity data points is of $0.3 \, \mathrm{m\,s^{-1}}$, to which $0.7 \, \mathrm{m\,s^{-1}}$ have been added quadratically in order to take into account possible instrumental and stellar noise.

The GLS periodogram shows several peaks well above noise at periods around 60 - 70 days (see Figure 12). The dashed and the dotted lines indicate a false-alarm probability of 1% and 10%, respectively. The mentioned peaks clearly exceed this level. The three highest peaks are found at 58, 69 and 85 days period, which are the yearly alias of each other. The peak at 58 days is the strongest of the series, however. Furthermore, there is significant excess power around 300 days period at above. In the same figure we plot for comparison the GLS periodogram of the activity indicator $logR'_{HK}$ and of the line bisector BIS. The former does not show any excess power at periods between 50 and 100 days. Instead, the excess power observed at periods above 300 days in the radial velocities seem

Table 4. Orbital and physical parameters of the planets orbiting HD 20794, as obtained from a three-Keplerian fit to the data. Error bars are derived from the covariance matrix. λ is the mean longitude ($\lambda = M + \omega$) at the given epoch.

Parameter	[unit]	HD 20794 b	HD 20794 c	HD 20794 d
Epoch	[BJD]	2'454'783.40362208		
i	[deg]	90 (fixed)		
V	[km s^{-1}]	87.9525 ($\pm$0.0001)		
P	[days]	18.315	40.114	90.309
		($\pm$0.008)	($\pm$0.053)	($\pm$0.184)
λ	[deg]	169.0	149.4	16.2
		($\pm$6.7)	($\pm$10.0)	($\pm$6.8)
e		0.0	0.0	0.0
		(fixed)	(*fixed*)	(*fixed*)
ω	[deg]	0.0	0.0	0.0
		(fixed)	(*fixed*)	(*fixed*)
K	[m s^{-1}]	0.83	0.56	0.85
		($\pm$0.09)	($\pm$0.10)	($\pm$0.10)
$m \sin i$	[$M_\oplus$]	2.7	2.4	4.8
		($\pm$0.3)	($\pm$0.4)	($\pm$0.6)
a	[AU]	0.1207	0.2036	0.3499
		($\pm$0.0020)	($\pm$0.0034)	($\pm$0.0059)
T_{eq}	[K]	660	508	388
N_{meas}		187		
Span	[days]	2610		
rms	[m s^{-1}]	0.82		
χ_r^2		1.39		

to follow the same pattern. The reason for this patter can be observed directly in the time domain (see Figure 11). In both $logR'_{HK}$ and line bisector *BIS* a long-term trend is observed most probably reflecting the magnetic cycle of the star. A similar trend, although with opposite sign and smaller amplitude, is observed in the radial-velocity data. From this fact we deduce that the power observed in the radial velocity at long periods is most probably caused by the stellar activity. We refer to Lovis et al. (2011a) for a general discussion in which also the specific case of HD 85512 is treated.

Given the absence of corresponding peaks in the activity indicator and the line bisector, we assume that the radial velocity signals at periods around 60 days are induced by a planetary companion. We have therefore fitted a single Keplerian to the radial-velocity data, but added also a second-degree polynomial to take into account the long-term variation induced by the stellar activity. The solution converges very rapidly and unambiguously towards a 58.4 days orbit. The activity signal is well fitted by a linear component of 0.5 m s^{-1}per year and a quadratic component of 0.14 m s^{-1}per year^2. The GLS periodogram of the residuals is very clean, as shown in Figure 14, since none of the peaks reaches the 10% false-alarm probability indicated by the dashed line. It must be noted all the original side peaks have disappeared and that our assumption them to be alias must have be correct.

The eventually obtained orbital parameters of HD 85512 b are given in Table 5 and the corresponding phase-folded radial-velocity curve is shown in Figure 13. The adopted period is $P = 58.4$ days. The eccentricity is clearly not significant, but given the large number of data points and the good convergence of the fit we have preferred to leave it as free parameter. The obtained value is of 0.11, but it must be recalled that setting it to zero would not at all change the quality of the solution. For the semi-amplitude we obtain the value of 0.77 m s^{-1}. The residual dispersion of the $N = 185$ data points around the fitted solution is of only 0.77 m s^{-1}. The reduced χ^2 is thus close to 1, indicating that the 0.7 m s^{-1}systematic error we added quadratically to the error bars may be a good estimate.

Using the previously determined parameters we can set the semi-major axis of the planetary orbit to 0.26 AU. For the minimum mass of the planet we obtain $m \sin i = 3.6[M_\oplus]$. The error on the mass due to only the fit uncertainties is of the order of 15%, despite the very low semi-amplitude. As in the case of the planets around HD 20794, this planet is possibly a super Earth, i.e a planet consisting to high degree by rocky material. Opposite to HD 20794, however, its parent star is much less luminous. The computed equilibrium temperature is of only 298 K, if we assume again an albedo of 0.3. This sets this possibly rocky planet at the inner edge of the habitable zone of its parent star.

In order to illustrate the cleanliness of the planetary radial-velocity signal and its poor correlation with the activity indicator we have detrended both series from the respective long-period signals. The results are best represented by the GLS periodogram in Figure 15. The top panel shows the radial-velocity signal, which, after detrending, appears even more clearly. The peak at 58 days is by far the strongest and the aliases show up at the expected periods with decreasing amplitude the further away from the main peak. Opposite, no such 'coherent' signal is observed in the log(R'_{HK}) at the mentioned periods, although
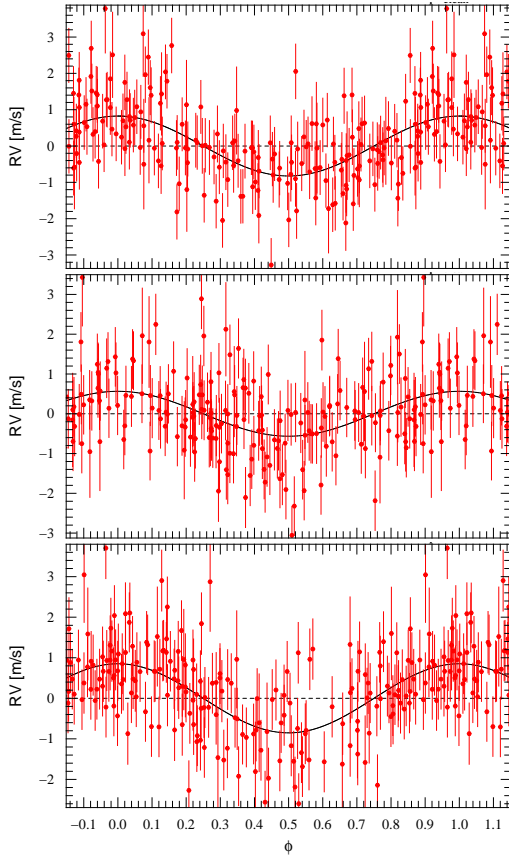
Fig. 10. Phase-folded RV data and fitted Keplerian solution for the three planetary components b, c and d of HD 20794 with $P = 18$ days, $P = 40$ days and $P = 90$ days, respectively. The dispersion of the residuals is of $0.82\,\mathrm{m\,s^{-1}}\,rms$.
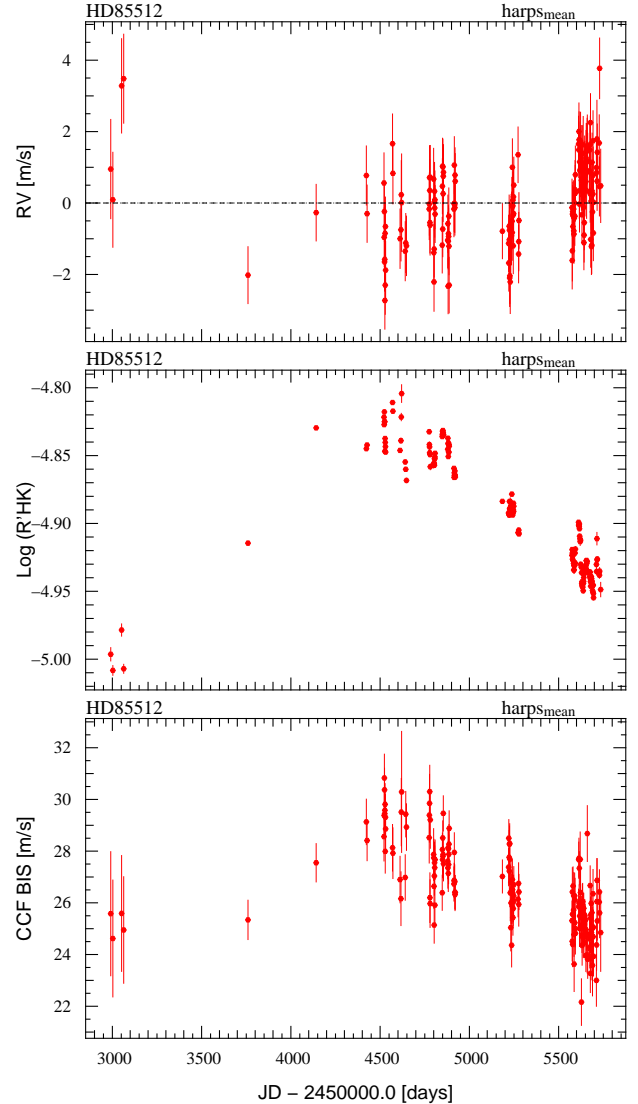

Fig. 11. Radial velocity, $\log(R'_{HK})$ and BIS of HD 85512 as a function of time. The dispersion of the 185 data points is of only $1.05\,\mathrm{m\,s^{-1}}\,rms$.

significant power is still present at various (shorter) periods. This excess power is actually also seen in the time series of $\log(R'_{HK})$, but the signal's amplitude, frequency and its phase is varying as a function of the observation epoch. We conclude that this signal is the expression of stellar rotation coupled with appearing and disappearing spots and plages, but that it cannot explain the presence of a a strong and coherent radial-velocity. This latter is therefore most likely due to a planetary companion.

5.3. The planetary system around HD 192310

Recently, Howard et al. (2010a) have announced the discovery of a Neptune-mass planet around HD 192310. Being part of the original HARPS GTO program and of our program, we have been observing this star for several seasons. The raw radial-velocity data of HD 192310 are shown in Figure 16. What strikes immediately is that, opposite to the previous objects presented in this paper, the dispersion of the 139 radial-velocity data points is of $2.6\,\mathrm{m\,s^{-1}}\,rms$ over the 6.5-years time span. The typical photon noise on the radial velocity data points is of $0.25\,\mathrm{m\,s^{-1}}$, to which, for the analysis, we add quadratically a noise of $0.7\,\mathrm{m\,s^{-1}}$ in order to account for possible instrumental and stellar noise.

The dispersion clearly exceeds the internal error and the stellar jitter expected for this quiet K3 dwarf. Even by eye one can recognize a rapid radial-velocity variation. The GLS periodogram (Figure 17) confirms the presence of a strong signal at about 74 days, which is exactly the period of the planet announced by Howard et al. (2010a). The dashed line indicates a false-alarm probability level of 1% but the $P = 74$ days signal exceeds this level by far. In the same figure we plot for comparison the GLS periodogram of the activity indicator $\log R'_{HK}$ and of the line bisector BIS. None of them reveals any significant power at the period indicated by the radial velocity.

The highest peak in the GLS periodogram for $\log(R'_{HK})$ would be observed at very long periods (> 1000 days) and is produced by the stellar magnetic cycle. We have therefore de-trended the data to better make appear short-period variations. Some excess power becomes then visible around 40 days. A closer look to the last observational season indeed reveals in the $\log(R'_{HK})$ time series a well established periodicity (Figure 18, top). The GLS periodogram of only these two
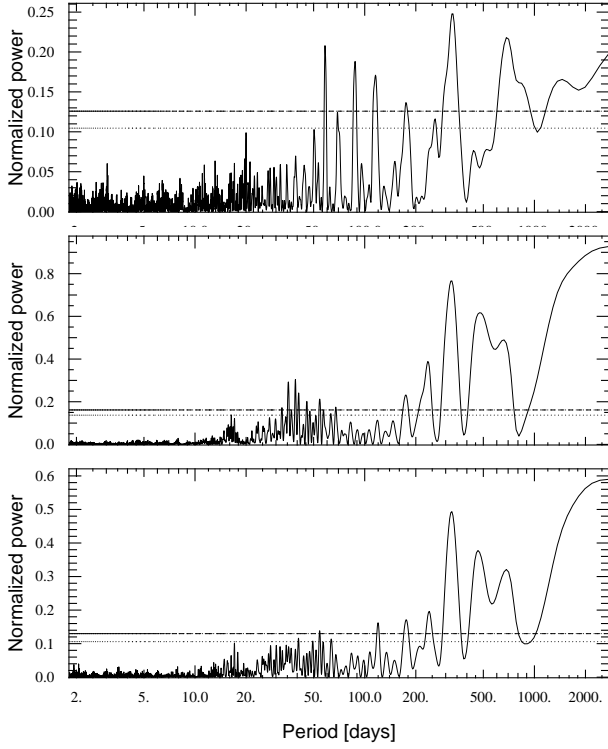
Fig. 12. GLS periodogram of the HD 85512 radial-velocity data with FAP levels at 10% and 1% level, respectively (top), the de-trended activity indicator $\log(R'_{HK})$ (center) and the line bisector (bottom).
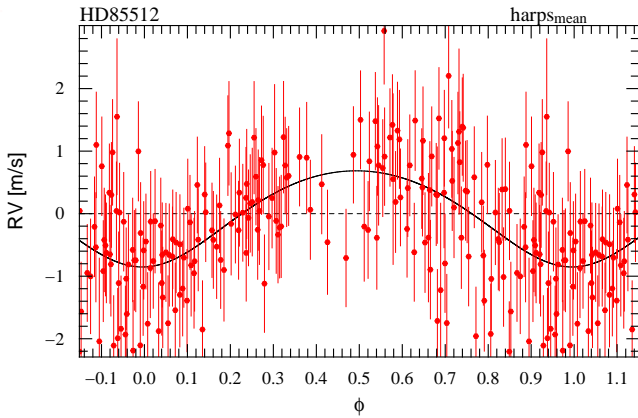

Fig. 13. Phase-folded RV data of HD 85512 and fitted Keplerian solution. The dispersion of the residuals is of $0.75\,\mathrm{m\,s^{-1}}\,rms$.
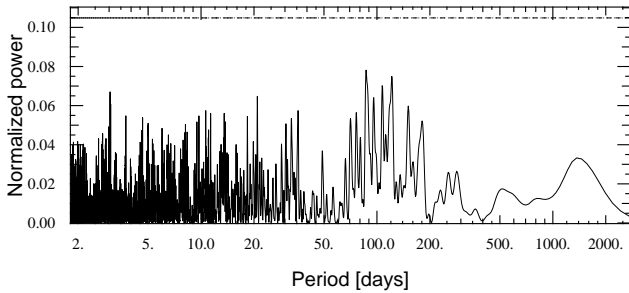

Fig. 14. GLS periodogram of the residuals to the $P = 58$ days best Keplerian fit to the HD 85512 RV data

Table 5. Orbital and physical parameters of the planets orbiting HD 85512 , as obtained from a Keplerian fit to the data. Error bars are derived from the covariance matrix. λ is the mean longitude ($\lambda = M + \omega$) at the given epoch.

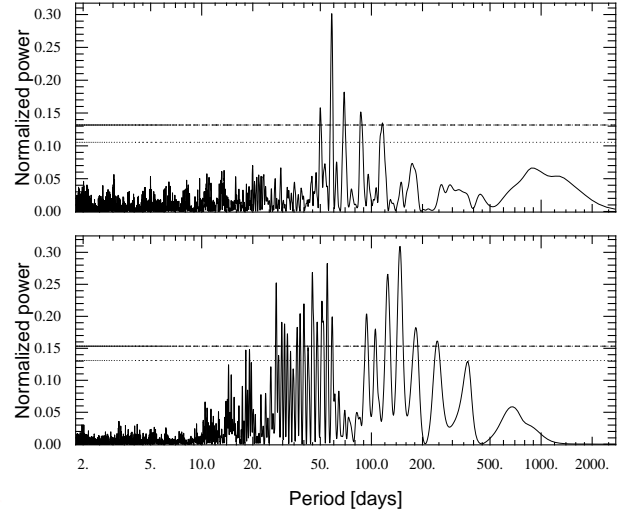| Parameter	[unit]	HD 85512 b
Epoch	[BJD]	2'455'239.70888680
i	[deg]	90 (fixed)
V	[km s^{-1}]	-9.4913 (±0.0038)
linear	[m s^{-1}/yr]	$+0.5085$ (±0.0003)
quadratic	[m s^{-1}/yr^2]	$+0.1423$ (±0.0002)
P	[days]	58.43
		(±0.13)
λ	[deg]	114.5
		(±6.3)
e		0.11
		(±0.10)
ω	[deg]	178
		(±0.58)
K	[m s^{-1}]	0.769
		(±0.090)
$m\sin i$	[$M_\oplus$]	3.6
		(±0.5)
a	[AU]	0.26
		(±0.005)
T_{eq}	[K]	298
N_{meas}		185
Span	[days]	2745
rms	[m s^{-1}]	0.77
χ^2_r		1.00

Fig. 15. Top: GLS periodogram of the de-trended radial velocities of HD 85512. Bottom: GLS periodogram of the detrended activity indicator $\log(R'_{HK})$

seasons indeed reveals a series of significant peaks centered at 40 to 45 days (Figure 18, bottom). It should be noted that this peak is most likely linked to the rotational period of the star and delivers therefore a direct and precise measurement of the stellar rotational period. Indeed, the so obtained period
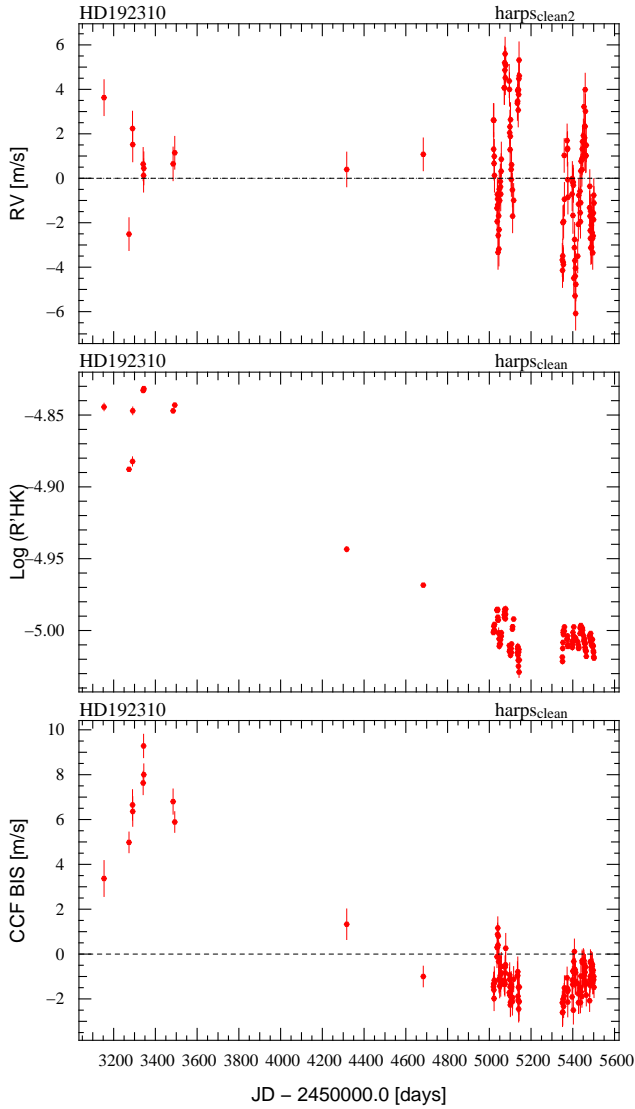
Fig. 16. Radial velocity, $\log(R'_{HK})$ and *BIS* of HD 192310 as a function of time. The dispersion is of the raw data is 2.6 m s^{-1} *rms*.
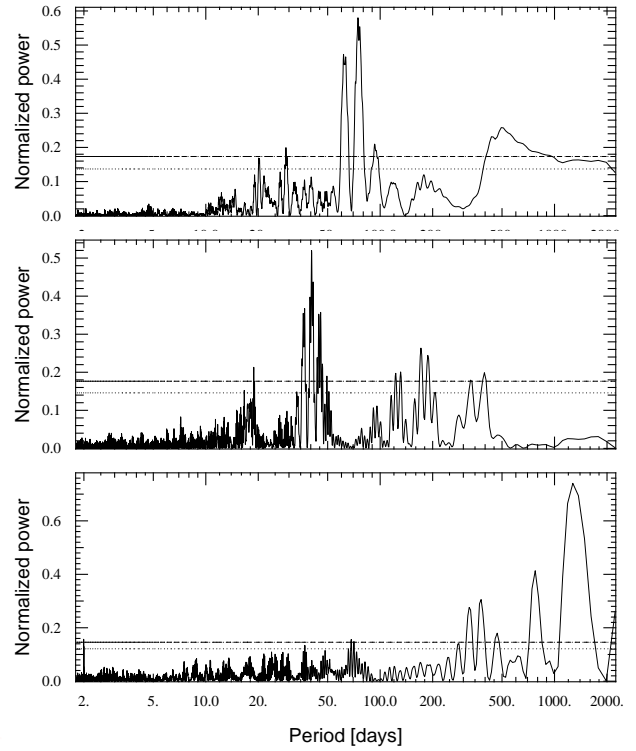

Fig. 17. GLS periodogram of the HD 192310 radial-velocity data with FAP levels at 10% and 1% level, respectively (top), the de-trended activity indicator $\log(R'_{HK})$ (center) and the line bisector (bottom). While a very clear peak appears at $P = 74$ days for the radial velocities, no such signal is present in the two other observables.

matches well the value computed using directly the value of $\log(R'_{HK})$ and indicated in Table 3. On the contrary, a complete lack of power is observed at the $P = 74$ days period, such that we can exclude any relation with the radial-velocity peak.

We have therefore fitted a Keplerian signal to the raw data and obtained a solution almost identical to that presented by Howard et al. (2010a). However, we considered this to be an intermediate solution, as suggested by the GLS periodogram of the residuals to the one-Keplerian solution (Figure 20). In fact, a significant power peak is left over at a period around 500 days. Although there is no direct correspondence with the peaks in the bisector and $\log(R'_{HK})$ power spectra, one may suspect that the residual radial-velocity signal is produced by stellar activity. Therefore, we have tested the correlation between the residuals to the one-Keplerian solution, on the one hand, and the line bisector and the $\log(R'_{HK})$, on the other hand. It shall be noted that this time the raw (not de-trended) $\log(R'_{HK})$ data where used, in order to identify possible long-period correlations. Figure 19 shows the complete absence of

correlation between these quantities, Pearson's correlation coefficient being close to zero in both cases. We conclude that the residual radial velocity variations are probably due to a second planetary companion at longer period. A closer look to the raw radial-velocity data of Figure 16 reveals actually a significant decrease in radial-velocity between the two last seasons, which, on the other hand, show both a trend upward. This should have suggested to us a second periodicity of 400 to 600 days.

Based on the previous considerations, we have fitted two Keplerians to the radial velocities of HD 192310 letting all the parameters free. The solution converges very rapidly and unambiguously towards a period of about 74.7 days and another of 526 days. The respective semi-amplitudes are of 3.0 m s^{-1} and 2.3 m s^{-1}, and the eccentricities of 0.13 and 0.32. The eccentricity of the second planet is significant at a 3-σ level, and we have therefore decided to let both the eccentricities as free parameter. The eventually obtained orbital parameters are given in Table 6 and the corresponding phase-folded radial-velocity curve is shown in Figure 21. The GLS of the residuals to the two-Keplerian does not show any significant peak (lower panel of Figure 20).

For the $N = 139$ data points we obtain a residual dispersion around the two-Keplerians solution of 0.92 m s^{-1}. The reduced χ^2 is 1.66. The uncertainty on the orbital period and the semi amplitude for the $P = 74$ days planet result to be very low. For the longer-period planet, the error is somewhat larger on the semi-amplitude, which is mainly linked to the uncer-
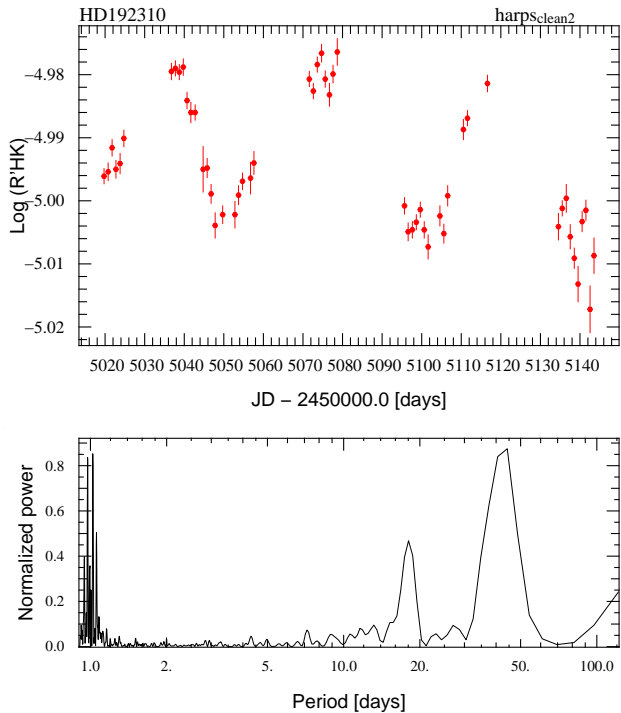
Fig. 18. Top: $\log(R'_{HK})$ time series of the two last observational seasons of HD 192310 . Bottom: Corresponding GLS periodogram

Fig. 19. Correlation plot of the residuals of the one-Keplerian fit to the radial velocities of HD 192310 versus the line bisector and the activity indicator $\log(R'_{HK})$, respectively

tainty on the eccentricity, which is in turn given by the lack of data points in the (short) descending slope of the radial-velocity curve. Period and eccentricity of the b component are, within the error bars, identical to the values given Howard et al. (2010a). The semi-amplitude – and thus the companion's mass – is different however at a level of 2-3 sigmas. This difference may be explained, on the one hand, by the fact that the second planet has not been detected by Howard et al. (2010a). On the other hand, it may simply be due to the higher uncertainty (0.4 m s^{-1} on K given by Howard et al. (2010a)), which is in turn due to the higher errors on the HIRES data: Indeed, when fitting two planets to both data sets simultaneously by adding on both a systematic error of 1.5 m s^{-1}, the residual dispersion of the HIRES data is of 1.8 m s^{-1}, while on the HARPS data the dispersion is only of 1 m s^{-1}. We conclude that we can undoubtedly confirm the planet HD 192310 b announced by Howard et al. (2010a) but suggest a correction of the semi-amplitude and thus its minimum mass.

The semi-major axis of the planetary orbits are 0.32 AU and 1.18 AU. For the minimum mass of the planets we obtain $m_b \sin i = 16.9 [M_\oplus]$ and $m_c \sin i = 23.4 [M_\oplus]$. The error on the mass due to only the fit uncertainties is of the order of 6% and 20%, respectively. While for the 74 days period planet the mass is quite well-determined thanks to the significant RV amplitude, for the long-period planet the uncertainty is rather large, mainly due to a lack of coverage over the steeply descending orbital phase portion. Given their mass and period both planets are probably of Neptune's composition. The equilibrium temperature defined by a Bond albedo of 0.3 is of the order of 355 K and 185 K, which places the two planets at the inner, respectively outer edge of the habitable zone of HD 192310.
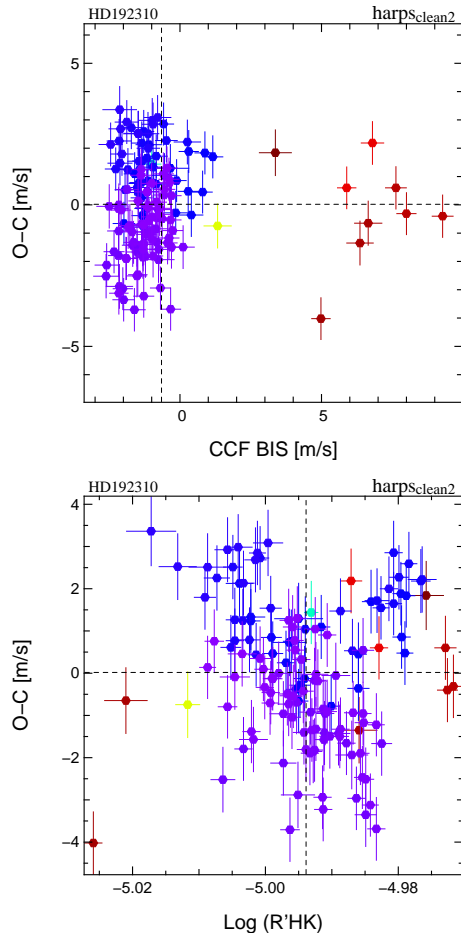
6. Discussion

6.1. Frequency of low-mass planets

By down-selecting our small sample of stars in terms of measured 'raw' RV dispersion, we have explicitly excluded the possibility of finding planets typically found by ongoing RV surveys. We have actually reduced the probability of finding any kind of planet in our program. On the other hand, the absence of more massive planets on short and intermediate orbits leaves free space for low-mass planets, possibly in the habitable zone, which is precisely what we are looking for. We have then optimized the observations to increase the probability for success by choosing the best possible instrument, selecting bright and inactive stars, and by optimizing the observation sampling and time span. Finally it should be noted that, when down-selecting from the original HARPS high-precision sample, we did not select on spectral type or other criteria that may favor or penalize the presence of planets.

Under these conditions we have found that at least 3 out of the 10 stars observed within our program harbor low-mass planets. Although statistics is poor over only ten targets, it is interesting to note that this 30% value was already announced by Lovis et al. (2009) who based their analysis on the larger
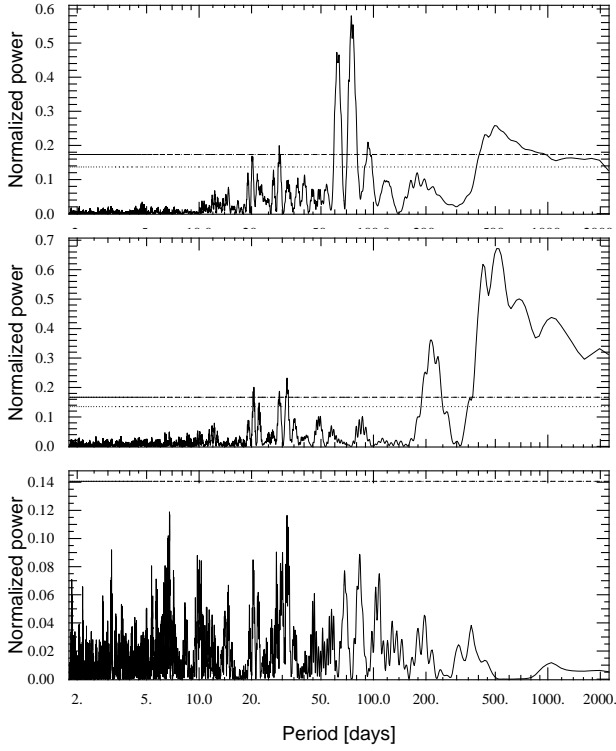
Fig. 20. From top to bottom the GLS periodograms of a) the RVs of HD 192310, b) the residuals to the one-Keplerian solution and c) the residuals to the two-Keplerian solution. FAP levels of 10% and 1% level are indicated apart from the last plot, where only the 10% level is shown.

Table 6. Orbital and physical parameters of the planets orbiting HD 192310, as obtained from a two-Keplerian fit to the data. Error bars are derived from the covariance matrix. λ is the mean longitude ($\lambda = M + \omega$) at the given epoch.

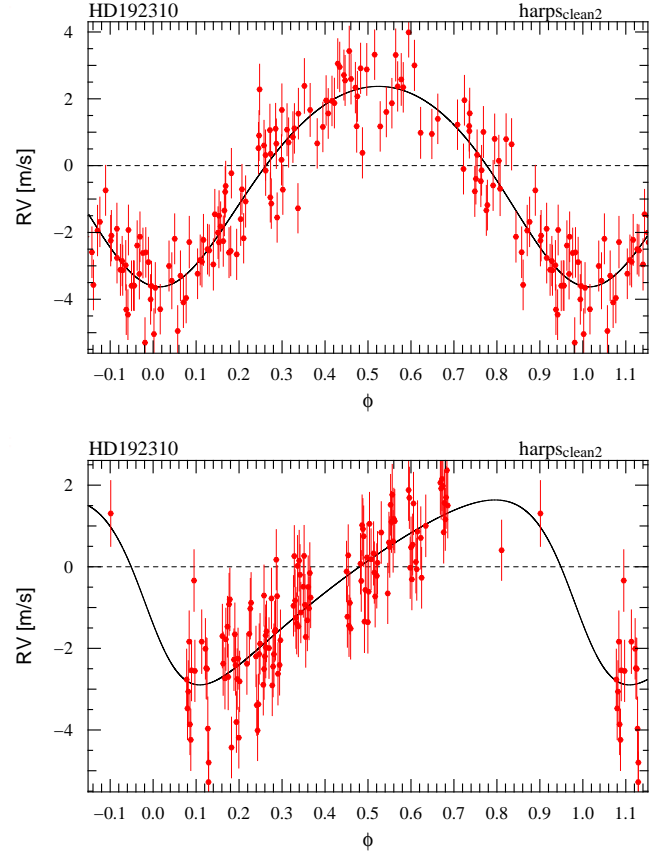| Parameter	[unit]	HD 192310 b	HD 192310 c
Epoch	[BJD]	2'455'151.02574596	
i	[deg]	90 (fixed)	
V	[km s^{-1}]	-54.2232 (±0.0003)	
P	[days]	74.72	525.8
		(±0.10)	(±9.2)
λ	[deg]	340.8	1.9
		(±2.3)	(±12.3)
e		0.13	0.32
		(±0.04)	(±0.11)
ω	[deg]	173	110
		(±20)	21
K	[m s^{-1}]	3.00	2.27
		(±0.12)	(±0.28)
$m \sin i$	[$M_\oplus$]	16.9	24
		(±0.9)	(±5)
a	[AU]	0.32	1.18
		(±0.005)	(±0.025)
T_{eq}	[K]	355	185
N_{meas}		139	
Span	[days]	2348	
rms	[m s^{-1}]	0.92	
χ_r^2		1.66	

Fig. 21. Phase-folded RV data of HD 192310 and fitted Keplerian solution for the two planetary companions with $P = 75$ days and $P = 526$ days, respectively. The dispersion of the residuals is of 0.91 m s^{-1} *rms*.

(< 200 stars) HARPS high-precision program. Theoretical works by Mordasini et al. (2009) actually forecasted that the frequency of small Neptunes and super-Earths on short and intermediated orbits would be considerably higher than that of Saturns and Jupiters. The recent amazing discoveries made by the KEPLER satellite using the transit technique further strengthen this fact. Borucki et al. (2011) report that the probability of finding low-mass planets is considerably higher than for Jupiter or Saturn-mass planets. Furthermore, when summing up the frequency of finding a planet of any mass, they end up with a probability of about 30%, again in perfect agreement with the results of Lovis et al. (2009). Opposite, there is partial disagreement between the HARPS results, on the one side, and the results by Howard et al. (2010b) and Howard et al. (2011), on the other side, who both claim that the total planet occurrence is of the order of 15%. It has to be mentioned, however, that the studies were restricted to stars with given spectral type and to planets with an upper period limit, and that the detection biases for low planetary masses and radii leave quite some room for making the different values compatible.

The fact that these low-mass planets were hardly found by the RV technique before, was probably simply due to a 'threshold effect' arising from the reduced precision and sometimes poor time sampling of existing instruments, which had a

hard time in detecting signals of few $m\,s^{-1}$ or even sub- $m\,s^{-1}$. HARPS has produced impressive results by exploring this previously unexplored domain. The number and quality of new low-mass planets is amazing, and many more are still to come. In fact, the detection of such small signals is not only a matter of precision but also of observation strategy and time span. Furthermore, complementary analysis is particularly important if one wants to exclude that the RV signal is produced by stellar noise. Systematic long-term follow-up is required. We refer here to Mayor (2011) for an overview and a summary of the outcomes of the HARPS program as a whole.

6.2. Nature of found planets

Radial velocities only provide minimum mass of the planets and contain no information on their radii. The mean density - and thus an indication on the composition of the planets - can only be determined by combining RVs and transit measurements. Some specific discoveries as for instance GJ 1214 b (Charbonneau et al. 2009), COROT-7 b (Léger et al. 2009; Queloz et al. 2009), KEPLER-10 b (Batalha et al. 2011) have shown that these low-mass planets have mean densities similar to our Earth and that they are probably made of rocky material. On the other hand, the atmosphere of planets on such short orbit (days) may have been evaporated by the star, opposite to planets on wider orbits. KEPLER discoveries of small planets on longer-period orbit (Lissauer et al. 2011) have indeed shown that their average density is generally lower than in the previous mentioned cases. One possible explanation is that they may have at least kept a thick gaseous envelope. By construction of our program, we have found planets of low-mass and on not too short-period orbits. Using the previous references we conclude that the presented planets are probably rocky or at least composed to a large extent of rocky material, but may have a thick atmosphere. An exception in our sample is constituted by HD 192310, which represents rather a 'classical' system of two Neptune-mass planets on long-period orbits.

In the case of HD 20794 actually all the found planets have masses in the domain of super-Earths and are probably rocky. Unfortunately, the period of the outermost planet is slightly too short to place it in the habitable zone of its star. Nevertheless, this particular example illustrates best the potential of our program and the fact that already today it is possible to find rocky planets in the habitable zone of solar-type stars.

The system of HD 85512 is much simpler in terms of dynamics, given the single planet, and does not deserve therefore any particular discussion. For this K5 dwarf the habitable zone is much closer in than for HD 20794. The planet's equilibrium temperature supposing an albedo of 0.3 is of the order of 298 K. This value is slightly higher than that of the Earth and places the planet just at the inner edge of the habitable zone (Selsis et al. 2007). On the other hand, we might expect a thick atmosphere for this planet. In the case the albedo would be higher, the equilibrium temperature would decrease. However, depending on the atmosphere's composition, the planet may also run into a runaway greenhouse effect (Selsis et al. 2007). Opposite, if its atmosphere is water-poor (in the case of a 'dry planet'),

the habitable zone happens to be much closer in (Abe et al. 2011). As the detail depends on many unknown parameters, it would be pure speculation to conclude on the habitability of this planets. Nevertheless, we shall note that HD 85512 is the lowest-mass planet discovered by RVs so far possibly lying in the habitable zone of its star.

6.3. Limits and possibilities of the ongoing program

The HARPS spectrograph allows us to find planetary companions to solar-type stars which induce sub meter-per-second radial velocity signatures. This proves two facts: a) Instrument precision is on short *and* long term below $1\,m\,s^{-1}$. b) For well-selected stars the stellar 'jitter', i.e. the sum of pulsation, granulation at all time scales, and activity, does not exceed $1\,m\,s^{-1}$.

In order to illustrate the achieved overall precision we have analyzed the residuals to the orbital solution of HD 20794 in more details. Figure 22 (upper panel) shows the residuals of the data to the three-Keplerian solution. Although some structure is identified in the early phases (data from the original HARPS GTO program) no secular trend at the sub- $m\,s^{-1}$ level is found over 7 years of observations. It has to be mentioned that the observation strategy has been improved the time sampling increased on the mentioned object in the frame of the HARPS-Upgrade GTO, which was specifically designed to obtain the best possible RV performance. The results are best illustrated by (Figure 22, lower panel), where the dispersion of the residuals is shown as a function of binning period for the last two years of observation (optimized strategy). For no binning (1 day bin) we obtain the mentioned scatter of $0.82\,m\,s^{-1}\,rms$. When increasing the binning, the dispersion decreases with the bin size, demonstrating that most of the noise is indeed averaged away. The noise decreases however with the power of -0.37, therefore different from 'white noise', which is expected to decrease as the square root of the bin size. This shows that the noise is not completely uniformly distributed over the frequency domain. Nevertheless, we end up with a scatter of only $0.2\,m\,s^{-1}$ when averaging over the timescale of a month.

In interesting to note that the stellar noise has a 'color', which reveals itself best in the GLS periodograms of $\log(R'_{HK})$ and BIS. If detected in the RV data (by comparing the frequency with $\log(R'_{HK})$ and BIS data, it could be 'filtered', or, in worst case, used to identify radial-velocity signals of same frequency and possibly induced by the star. In the former case, one could actually benefit from the fact that the noise is colored to improve the RV data and reduce the error bars on the planets fitted parameters. This is easily done when the frequency of the planet signal is significantly different from the frequency detected in $\log(R'_{HK})$ and BIS, supposing that possible stellar jitter would appear at similar frequencies (or harmonics of them) as for the activity indicator and the line bisector. Filtering of the unwanted frequencies could be done in the Fourier domain, for instance. Alternatively, we propose to fit the planet orbital signal convolved with the window function directly in the Fourier domain.

As mentioned above, and as we did in the present paper, the activity indicator and the line bisector may be used for 'mon-
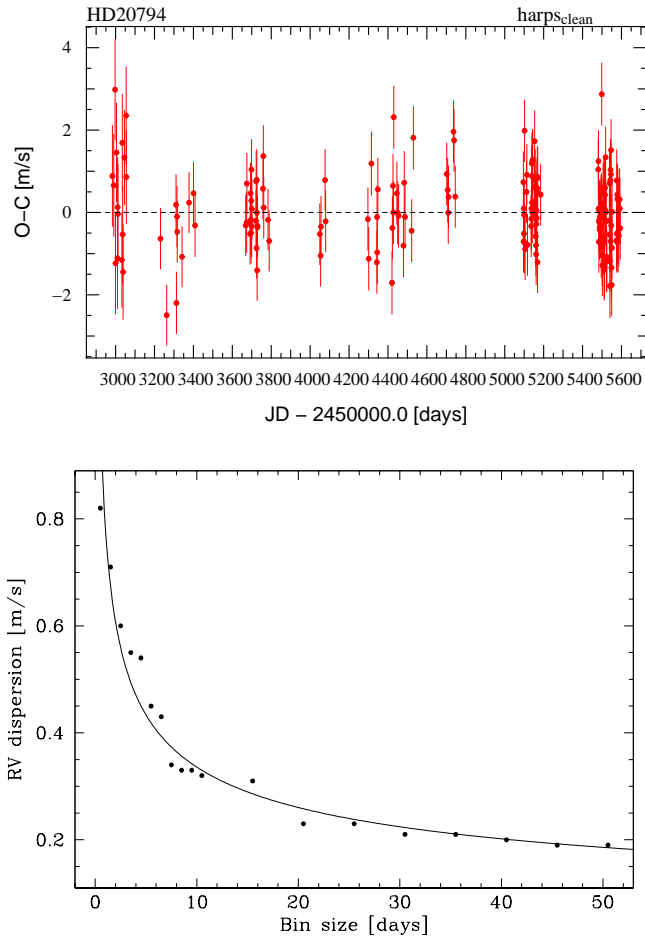
Fig. 22. Top: Residuals of the radial velocities of HD 20794 to the three-Keplerian fit as a function of time. Bottom: Allen analysis of the dispersion of these same residuals over the past two years.

itoring' and detecting possible correlations among the various observables. If we assume that RV jitter caused by stellar noise should appear at the same frequencies (or harmonics) as for the activity indicator and the line bisector, then we can use this information to detect 'suspect' signals. It must be pointed out, however, that both indicators remain a diagnostic rather than a proof for the presence or absence of induced RV signal, and this fact is best illustrated by two extreme examples: a) If no signal is detected in the *BIS*, one cannot exclude that the observed RV signal would *not* be induced by the star, as demonstrated by Santos et al. (2003). b) The cases of HD 85512 and HD 192310 show very nicely that, despite the presence of a long-term signal in the $\log(R'_{HK})$, no correlated signal is observed in the RV. This confirms the conclusions drawn by Santos et al. (2010) who did not find any evidence for radial-velocity variations induced by variations of the stellar magnetic cycle with amplitudes significantly above $1 \, \text{m s}^{-1}$ for early K-type stars.

$\log(R'_{HK})$ and *BIS* are thus excellent diagnostic parameters, provided that they are determined to sufficient precision level. Thanks to the spectroscopic stability of HARPS both can be determined to extreme accuracy. For the line bisector we have demonstrated that it can be even more stable than the RV itself, because it is only affected by asymmetry changes. The

$\log(R'_{HK})$, on the other hand, can be measured to the milli-dex precision, a level at which one actually has hard time to distinguish stellar effects from instrument effects. An interesting side product of this is the direct determination of the stellar rotational velocity, which, for all the three cases presented here, turned out to be in excellent agreement with the value directly derived from $\log(R'_{HK})$ using the procedures given by Mamajek & Hillenbrand (2008). The changes made recently on the HARPS data-reduction pipeline have greatly contributed to the improved spectroscopic performances of HARPS (Lovis et al. 2011a).

7. Conclusions

Of the original HARPS high-precision program we have chosen ten bright and quiet stars to be followed-up in the frame of the HARPS-Upgrade GTO program. These stars were furthermore selected because they were showing very small radial-velocity dispersion, from which we could exclude the presence of massive and/or short-period planets. The goal of this program is to search for low-mass, possibly rocky planets in the habitable zone.

Despite this severe 'down-selection', we have found that at least three out of the ten stars harbor low-mass planetary companions. Around HD 192310 we could confirm the Neptune-mass planets recently announced by Howard et al. (2010a), but identified a second companion of similar mass on a much wider orbit and lying at the outer edge of the habitable zone. In addition, a planet of only $m \sin i = 3.6 [M_\oplus]$ was found to orbit the star HD 85512. Due to the late spectral type of this star the $P = 58$ days-orbit planet of probably rocky nature lies at the inner edge of its habitable zone. Finally, we reported the system around HD 20794 consisting of three super-Earths of only few Earth-masses each. While the two signals at 18 and 90 days period leave little doubt on their planetary nature, we will need further data to definitively confirm the $m \sin i = 2.4 [M_\oplus]$ on the $P = 40$ days orbit. It must be noted, however, that the semi-amplitude induced by this planet on its parent star is of only $0.56 \, \text{m s}^{-1}$, the smallest planetary signature ever detected. All these discoveries were made possible thanks to the ultra-precise radial velocities and the impressive measurements of the line bisector and the $\log(R'_{HK})$ delivered by the HARPS instrument.

Present and future discoveries of such low-mass planets will be of great importance per se, pushing the variety of known extrasolar planets one step further. They will furthermore offer, thanks to the proximity and magnitude of their parent star, an excellent opportunity for precise and in-depth photometric, polarimetric, spectroscopic and astrometric follow-up of the planet and its host star. A bunch of exciting and unprecedented observational data will follow, providing new inputs to the formation models and the understanding of the internal structure and the atmosphere of these planets. Finally, these candidates will be among the best targets to be considered by future space missions, which will need appropriate targets to look at and will have to take the best advantage of observational time.

References

Abe, Y., Abe-Ouchi, A., Sleep, N. H., & Zahnle, K. J. 2011, Astrobiology, 11, 443

Alibert, Y., Mordasini, C., & Benz, W. 2011, A&A, 526, A63+

Andrae, R., Schulze-Hartung, T., & Melchior, P. 2010, ArXiv e-prints

Batalha, N. M., Borucki, W. J., Bryson, S. T., et al. 2011, ApJ, 729, 27

Borucki, W. J., Koch, D. G., Basri, G., et al. 2011, ApJ, 728, 117

Butler, R. P., Vogt, S. S., Marcy, G. W., et al. 2004, ApJ, 617, 580

Casagrande, L., Portinari, L., & Flynn, C. 2006, MNRAS, 373, 13

Charbonneau, D., Berta, Z. K., Irwin, J., et al. 2009, Nature, 462, 891

Dumusque, X., Santos, N. C., Udry, S., Lovis, C., & Bonfils, X. 2011a, A&A, 527, A82+

Dumusque, X., Udry, S., Lovis, C., Santos, N. C., & Monteiro, M. J. P. F. G. 2011b, A&A, 525, A140+

ESA. 1997, The HIPPARCOS and TYCHO catalogue, ESA-SP 1200

Howard, A. W., Johnson, J. A., Marcy, G. W., et al. 2010a, ArXiv e-prints

Howard, A. W., Marcy, G. W., Bryson, S. T., et al. 2011, ArXiv e-prints

Howard, A. W., Marcy, G. W., Johnson, J. A., et al. 2010b, Science, 330, 653

Ida, S. & Lin, D. N. C. 2008, ApJ, 685, 584

Léger, A., Rouan, D., Schneider, J., et al. 2009, A&A, 506, 287

Lissauer, J. J., Fabrycky, D. C., Ford, E. B., et al. 2011, Nature, 470, 53

Lovis, C. 2011, in prep.

Lovis, C., Dumusque, X., Santos, N. C., et al. 2011a, ArXiv e-prints

Lovis, C., Mayor, M., Bouchy, F., et al. 2009, in IAU Symposium, Vol. 253, IAU Symposium, 502–505

Lovis, C., Mayor, M., Pepe, F., et al. 2006, Nature, 441, 305

Lovis, C., Ségransan, D., Mayor, M., et al. 2011b, A&A, 528, A112+

Mamajek, E. E. & Hillenbrand, L. A. 2008, ApJ, 687, 1264

Mayor, M., Bonfils, X., Forveille, T., et al. 2009a, A&A, 507, 487

Mayor, M., Pepe, F., Queloz, D., et al. 2003, The Messenger, 114, 20

Mayor, M., Udry, S., Lovis, C., et al. 2009b, A&A, 493, 639

Mayor, M. e. a. 2011, in prep.

McArthur, B. E., Endl, M., Cochran, W. D., et al. 2004, ApJ Letters, 614, L81

Mordasini, C., Alibert, Y., & Benz, W. 2009, A&A, 501, 1139

Neves, V., Santos, N. C., Sousa, S. G., Correia, A. C. M., & Israelian, G. 2009, A&A, 497, 563

Pepe, F., Correia, A. C. M., Mayor, M., et al. 2007, A&A, 462, 769

Queloz, D., Bouchy, F., Moutou, C., et al. 2009, A&A, 506, 303

Santos, N. C., Bouchy, F., Mayor, M., et al. 2004, A&A, 426, L19

Santos, N. C., Gomes da Silva, J., Lovis, C., & Melo, C. 2010, A&A, 511, A54+

Santos, N. C., Mayor, M., Naef, D., et al. 2002, A&A, 392, 215

Santos, N. C., Udry, S., Mayor, M., et al. 2003, A&A, 406, 373

Selsis, F., Kasting, J. F., Levrard, B., et al. 2007, A&A, 476, 1373

Sousa, S. G., Santos, N. C., Mayor, M., et al. 2008, A&A, 487, 373

Torres, G., Andersen, J., & Giménez, A. 2010, A&A Rev., 18, 67

Udry, S., Bonfils, X., Delfosse, X., et al. 2007, A&A, 469, L43

Udry, S. & Mayor, M. 2008, in Astronomical Society of the Pacific Conference Series, Vol. 398, Astronomical Society of the Pacific Conference Series, ed. D. Fischer, F. A. Rasio, S. E. Thorsett, & A. Wolszczan, 13–+